



CHORUS

This is the accepted manuscript made available via CHORUS. The article has been published as:

Complex vibrations in arsenide skutterudites and oxyskutterudites

F. Bridges, B. Car, L. Sutton, M. Hoffman-Stapleton, T. Keiber, R. E. Baumbach, M. B. Maple, Z. Henkie, and R. Wawryk

Phys. Rev. B **91**, 014109 — Published 22 January 2015

DOI: [10.1103/PhysRevB.91.014109](https://doi.org/10.1103/PhysRevB.91.014109)

Complex Vibrations in Arsenide and Oxy-Skutterudites

F. Bridges,¹ B. Car,¹ L. Sutton,¹ M. Hoffman-Stapleton,¹ T. Keiber,¹
R. E. Baumbach*,² M. B. Maple,² Z. Henkie,³ and R. Wawryk³

¹*Physics Department, University of California, Santa Cruz, California 95064, USA*

²*Physics Department, University of California, San Diego, California, USA**

³*Institute of Low Temperature and Structure Research,
Polish Academy of Sciences, 50-950 Wrocław, Poland*

(Dated: December 17, 2014)

The local structure of two skutterudite families - CeM_4As_{12} ($M = Fe, Ru, Os$) and $LnCu_3Ru_4O_{12}$ ($Ln = La, Pr, \text{ and } Nd$) - have been studied using the Extended X-Ray Absorption Fine Structure (EXAFS) technique with a focus on the lattice vibrations about the rare earth “rattler atoms”, and the extent to which these vibrations can be considered local modes, with the rattler vibrating inside a nearly rigid cage. X-ray absorption data at all the metal edges were collected over a temperature range of 4 to 300 K and analyzed using standard procedures. The pair-distances from EXAFS results agree quite well with the average structure obtained from diffraction. The cage structure is formed by the M and As atoms in CeM_4As_{12} and by Cu, O, and Ru atoms in $LnCu_3Ru_4O_{12}$. Although some of the bonds within the cage are quite stiff (Correlated Debye temperatures, θ_{CD} , are ~ 500 K for CeM_4As_{12} and above 800 K for $LnCu_3Ru_4O_{12}$) we show the structure is not completely rigid. For the rattler atom the nearest neighbor pairs have a relatively low Einstein temperature, θ_E ; ~ 100 -120 K for Ce-As and ~ 130 K for Ln -O. Surprisingly, the behavior of the second neighbor pairs are quite different; for CeM_4As_{12} the second neighbor pairs (Ce- M have a weaker bond while for $LnCu_3Ru_4O_{12}$ the Ln -Ru second neighbor pair has a *stiffer* effective spring constant than the first neighbor pair. In addition, we show that the As_4 or CuO_4 rings are relatively rigid units and that their vibrations are anisotropic within these cubic structures, with stiff restoring forces perpendicular to the rings and much weaker restoring forces in directions parallel to the rings. Consequently vibrations of the rings may also act as “rattlers” and help suppress thermal conductivity. In general neither the rigid cage approximation nor the simple reduced mass approximation are sufficient for describing rattler behavior.

PACS numbers:

I. INTRODUCTION

The filled skutterudite, LnM_4X_{12} ($Ln = La, \text{ rare earth; } M = Fe, Ru, Os; X = P, As, Sb$) have been studied extensively for several decades, in large part due to the variety of ordered ground states that they exhibit and their good thermoelectric properties.¹⁻⁴ Significant attention has been given to their unusual structure, in which the Ln atom (e.g., La, Ce, Pr, etc.) is weakly bonded to the nearest neighbor X atoms that form a 12-neighbor surrounding cage in two of the unit cell sub-cubes (see Fig. 1:Left). In general, the cage structure formed from the X and M atoms (or Cu, O and M atoms in oxy-skutterudites) is assumed to be quite rigid. As a result of the weak bonding, the Ln atoms have large amplitude thermal vibrations and are hence called “rattler” atoms.^{5,6} These large amplitude vibrations strongly scatter phonons and lead to a very low lattice thermal conductivity, κ_l . In these materials, the electrical contribution, κ_e , to the total thermal conductivity, κ_{tot} , is usually small and the thermal conductivity is dominated by the lattice contribution. Many of these materials have semiconducting properties, with a moderate electrical conductivity, σ_e .^{3,7} Moreover, their Seebeck coefficient, S , is sometimes enhanced, owing to the strong hybridization between the conduction electron and f-electron states.⁷⁻¹⁰ Consequently, these materials have

good thermoelectric properties, parametrized by a high value of the figure of merit, $ZT = TS^2 \frac{\sigma_e}{\kappa_{tot}}$. Unlike typical metals, S can be large and the ratio $T\sigma_e/\kappa_{tot}$ is not approximately constant. Moreover, it has been shown that both n- and p-type components, which are necessary to construct a thermoelectric device, are readily made by the choice of rare earth - e.g., Ce and Yb.^{5,11,12}

The CeM_4As_{12} filled skutterudite compounds have been synthesized relatively recently and have not yet been extensively studied. As the pnictogen is varied from P to As to Sb,^{2,13} the lattice constant increases and the strength of the hybridization decreases, as reflected in the gap size for the semiconductors in this series of compounds.^{3,7} As such, the cerium-arsenide compounds have properties that are intermediate between the cerium-phosphide and the cerium-antimonide analogues. While $CeFe_4As_{12}$ exhibits semimetallic and semiconductor behavior that is finely tuned by morphology and charge carrier concentration,¹⁰ $CeRu_4As_{12}$ shows evidence for strong electronic correlations and non-Fermi-liquid behavior.⁸ In contrast, $CeOs_4As_{12}$ is a hybridization gap insulator with a gap size that is intermediate between those of $CeOs_4P_{12}$ and $CeOs_4Sb_{12}$.⁹ This compound was also recently proposed to be a possible candidate for topological insulating behavior.¹⁴ These three systems all exhibit enhanced thermoelectric properties, as evidenced in their large thermopower at low T;⁸⁻¹⁰

clearly they are attractive for thermoelectric applications at lower temperatures.

While most discussions of the rattler behavior in filled skutterudites focus on the environment immediately surrounding the lanthanide ion, it is important to note that the other six sub-cubes within the unit cell contain 4-atom, nearly square, rings of pnictide atoms (X), which may play an important role in the unusual lattice behavior. However, other than considering these rings as part of the rigid cage structure, they have been ignored. In order to develop an understanding of the relative importance of the extended lattice to the rattler behavior, it is useful to compare with closely related structures.

One such family of compounds are the oxy-skutterudite materials,¹⁵⁻²¹ $LnCu_3M_4O_{12}$ where Ln = rare earth atoms and also divalent and monovalent atoms, while M can be a range of metal atoms including Fe^{3+} , Ti^{4+} and Ru^{4+} .¹⁷ These materials are sometimes referred to as double perovskites,¹⁷ but because of the nearly identical structure to the filled skutterudites - see Fig. 1:Middle, we refer to them as oxy-skutterudites. Some of these materials have been studied over the last decade and have a range of interesting properties but there is little information about the local structure.¹⁸ In this case, the pnictide rings are replaced by a CuO_4 unit which appears quite rigid; we'll refer to these units as CuO_4 rings - see Fig. 1:Middle. There is some disagreement on the nature of the bonding of Cu; Hollmann *et al.*²¹ suggest that Cu forms a Cu^{2+} ion while Ramirez *et al.*¹⁶ suggest that Cu is Cu^{1+} ; Schwingenschlogl *et al.*²² propose a strong covalent bond between Cu and O. The CuO_4 rings are relatively larger in size than the pnictide rings, slightly more rectangular, and in most cases considerably lighter in mass. By comparing results for LnM_4X_{12} and $LnCu_3M_4O_{12}$, we are able to explore the extent to which these pnictide and CuO_4 rings play a role in the vibration properties of skutterudite compounds: i.e., to study the validity of the rigid cage model.

Under the rigid cage approximation, the rattler atom is vibrating inside a rigid box. In such a model, the vibrations of the rattler atom should be isotropic in all directions - i.e., the equation of motion is

$$M \frac{d^2 u}{dt^2} = -K_{\text{eff}} u. \quad (1)$$

Here u is any radial displacement of the rattler atom, K_{eff} , the effective spring constant is $4K_1 + 8/3K_2$ (where K_1 is the nearest neighbor direct spring constant and K_2 is the corresponding direct spring constant to the second neighbors), and the effective mass M is just the rattler mass when the cage is rigid. However, some have suggested²³ that one should still use the reduced mass for the $Ln-X$ pair (e.g., Ce-As). It is not clear which approximation is better if the cage is stiff but not rigid - possibly neither.

A further motivation for a more detailed investigation of such systems is that in a recent study²⁴ of $NdOs_4Sb_{12}$,

$PrOs_4Sb_{12}$, and $EuOs_4Sb_{12}$, the vibration amplitude of the rattler, relative to the first and second neighbors (i.e., Nd-Sb and Nd-Os pairs for $NdOs_4Sb_{12}$), did not increase at the same rate with temperature, which is inconsistent with a completely rigid cage model. The faster increase in vibration amplitude observed for the second neighbor pair Nd-Os may not be surprising if one assumes some motion of the Os atoms in the cage; however the Os-Os pair is quite stiff so how that occurs is not obvious. Further, there is an unusually large static distortion for the Nd-Os pair that is not well understood but may be related to a cage distortion.²⁴ For the oxy-skutterudites, as we'll show here, an even more surprising result is observed: the vibration amplitude for the second neighbor pair (e.g., the Nd-Ru in $NdCu_3Ru_4O_{12}$) increases *more slowly* with temperature than for the first neighbor pair Nd-O. That suggests a stiffer effective spring between Nd and Ru than between Nd and its closest neighbor, O. This prompted a closer look at the structure and particularly the motions of the pnictide and the CuO_4 rings.

In evaluating/comparing these EXAFS results with other types of measurements or calculations, two main points must be kept in mind. First, some measurements and corresponding calculations focus more on the mode energies, and for low dispersion modes a peak can be observed. Examples include inelastic neutron scattering for $La(Ce)Fe_4Sb_{12}$ ²⁵ where adding a rattler introduces a low dispersion mode, and nuclear resonant inelastic scattering²⁶ which shows well defined peaks corresponding to low dispersing phonon modes. However these modes are the collective motion of several atoms and in general do not probe the atoms involved directly, although in some cases one atom may dominate the response. Other types of experiments focus on the vibration amplitudes of pairs of atoms (EXAFS and neutron or X-ray pair distribution analysis) or vibration amplitudes of specific atoms (thermal parameters in diffraction); these vibrations are projections of many modes onto the atoms of interest - and the average vibration energy may not be the same as experiments that probe the phonon modes. A further difference between EXAFS and thermal parameters is that EXAFS probes correlated motions of the first few neighbors while the thermal parameters only parametrize the vibrations of a given atom. Consequently characteristic energies such as Einstein temperatures extracted from these types of measurements are not equal in general, but are often comparable. In the analysis of the atom-pair vibrations here, we use the Einstein and correlated Debye models; these are relatively simple approximations - but used extensively in the literature; since the vibration amplitude (σ^2) is an average over all modes and all of q-space, details are averaged out. Calculations from lattice dynamics studies generally do not report the correlated vibrations of specific atom pairs.

Here, we report Extended X-Ray Absorption Fine Structure (EXAFS) measurements on a series of As-skutterudites (CeM_4As_{12} ; $M = Fe, Ru, Os$) and oxy-

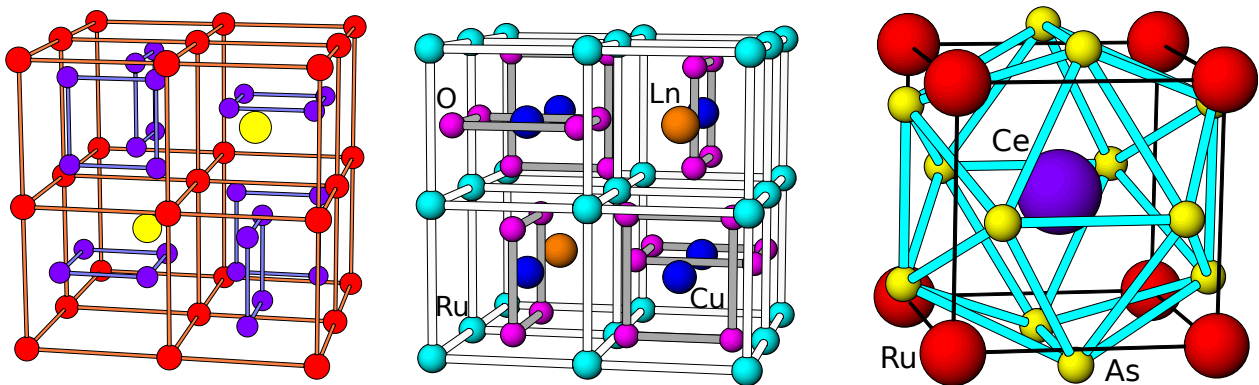


FIG. 1: (Color on-line) Left) The structure of CeM_4As_{12} ($M = Fe, Ru, Os$); the unit cell is cubic (space group $Im\bar{3}$). The M atoms are red, the Ce atoms are plotted in yellow (large), and the As atoms are purple (small). Within each unit cell there are eight sub-cubes formed by the M atoms; in six of these sub-cubes, there are nearly square rings formed by four As atoms, with a single Ce atom in the center of the other two sub-cubes. Middle) The similar structure for the oxy-skutterudites $LnCu_3Ru_4O_{12}$ ($Ln = La, Pr, \text{ and } Nd$). Here the pnictide rings are replaced by the CuO_4 rings. Right) The cage structure about the rattler atom; twelve As or O atoms form an icosahedron of nearest neighbors while eight transition metal atoms (M) form a cube of second neighbors.

skutterudites ($LnCu_3Ru_4O_{12}$; $Ln = La, Pr, \text{ and } Nd$), with particular attention paid to the first and second neighbor pairs about the rattler atoms. The results for the As- and oxy-skutterudites are quite different. We show that, in fact, the vibrations of the pnictide and CuO_4 rings are anisotropic with a small amplitude in one direction and a large amplitude in another direction. Although temperature dependencies are often reported in terms of an Einstein or correlated Debye temperature, EXAFS actually measures the effective spring constant, when in the high T limit;²⁷ we therefore also report effective spring constants for each pair in Sec. VIA, including pairs within the cage structure. The effective spring constant for vibrations in a given direction are crucial for understanding the vibrational properties of these systems. Based on our results, we discuss implications for understanding the rattling behavior in these and related compounds. Unfortunately, there are very few local structure studies of these systems with which to compare, and none have addressed the vibrations of the second neighbors about a rattler atom. We discuss these works briefly in Sec. VIB.

A. Effective Spring Constants

The vibration of an atom pair is determined by the direct spring constant between the two atoms, plus a network contribution from the surrounding springs and atoms. In EXAFS we measure the mean square displacement σ^2 for a given pair as a function of temperature, where σ is the width of the pair distribution function. This includes both static and thermal contributions to local disorder. In the high T limit thermal disorder dominates; the average thermal energy in the spring is $1/2 k_B T$ and the average potential energy is given by

$$\frac{1}{2}K_{\text{eff}} \langle u^2 \rangle = \frac{1}{2}K_{\text{eff}}\sigma^2 = \frac{1}{2}k_B T \quad (2)$$

where u is the net displacement from equilibrium for a pair of atoms and K_{eff} is the effective spring constant between them. Thus in the high T limit, K_{eff} is given by:²⁷

$$K_{\text{eff}} = \frac{k_B T}{\sigma^2}. \quad (3)$$

By extrapolating to high T we can obtain a good estimate of the effective spring constant. This works very well if the Einstein or correlated Debye temperatures are not much larger than 300 K, but for high Debye temperatures the uncertainty increases. Examples of such estimations of K_{eff} will be given following the EXAFS analysis.

II. EXPERIMENTAL DETAILS

A. Samples

Samples of the As-skutterudites were prepared and characterized as described in detail in references 8–10,13. The oxy-skutterudite samples were grown using a solid state reaction. The starting components, Ln_2O_3 , CuO , and RuO_2 powders, were first dried at 200 °C overnight to remove moisture and then mixed in stoichiometric amounts. Next the mixed powders were pressed into pellets and heated for 24 hours at 1050 °C. These pellets were reground, repressed, and refired several times. X-ray powder diffraction showed that by the 3rd firing almost all of the material reacted. A total of five firings

were done to ensure chemical homogeneity.

To prepare the samples for EXAFS data collection, they were first ground with a mortar and pestle and then filtered through a fine screen, limiting the size of the particles to $< 25 \mu$. This powder was lightly brushed onto Scotch tape[®]; in this process the larger particles are removed and the remaining particles are typically $\leq 5 \mu$ in size. Two pieces of tape were pressed together to encapsulate the powder and the double tape layers cut into thin strips, approximately 2 to 3 mm wide. These strips were stacked to give the thickness needed to yield an edge step-height of ~ 0.4 - 0.7 for the edge of interest. The small particle size and stacking of multiple layers results in very uniform sample thicknesses; in addition, the sample is scanned to find the region with the least spatial variation. Because of thermal expansion/contraction in the cryostat, this part of the sample must be found for each temperature.

B. Data Collection

EXAFS data were collected at the Stanford Synchrotron Radiation Lightsource (SSRL) for each metal atom in the samples. Details about the monochromators are provided in Table S1 in the Supplemental section. In each case the monochromator was detuned 50% to reduce harmonics. The samples were mounted in a helium flow cryostat to investigate the temperature dependence of the EXAFS, from 4-300 K. Most data were collected in transmission mode with the sample at 90° to the beam. However, the lanthanide L_{III} edges were collected in both fluorescence and transmission modes with the sample at 45° to the beam. For those lanthanide L_{III} edges for which the fluorescence data is better than the transmission data, a small self-absorption correction is automatically included in our code;²⁸ it is small but not completely negligible for the skutterudites - for example approximately 1.08 for the La L_{III} edge in $\text{LaCu}_3\text{Ru}_4\text{O}_{12}$.

The EXAFS data were reduced using standard procedures,²⁹ which includes a pre-edge background subtraction using the Victoreen equations for transmission data,³⁰ and a spline-fit of the post-edge background in order to extract the EXAFS oscillations, $\chi(E)$. This function was converted to a k -space function using the relation $k = \sqrt{(2m(E - E_o))/\hbar^2}$. Here E_o is the edge energy defined experimentally as the energy at the half-height point on the edge step. For additional details see reference 31.

Examples of the k -space EXAFS data, $k\chi(k)$, for the $\text{CeOs}_4\text{As}_{12}$ sample are shown in Fig. 2a. The two short scans (Ce and As) are limited by the Ce L_{II} and Os L_{III} edge's, respectively. Similar representative k -space data for one of the oxy-skutterudite samples, are shown in Fig. 2b. In all cases the quality of the data is high with little noise over the available k -range.

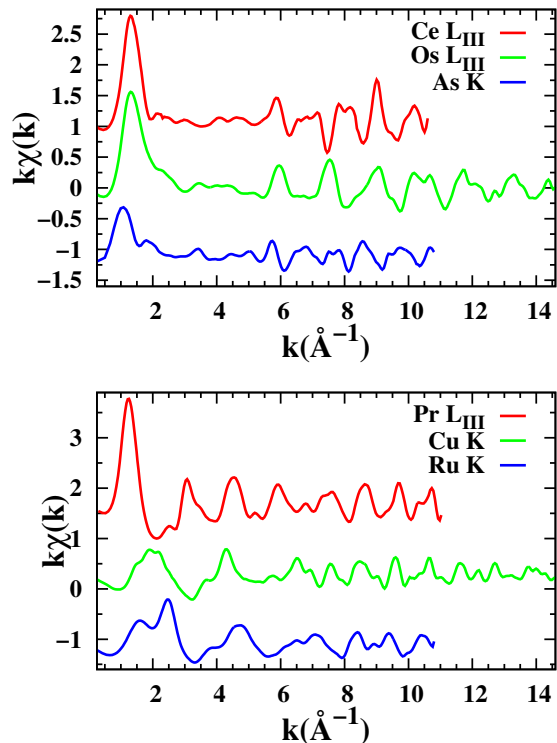


FIG. 2: (Color on-line) a) k -space data ($k\chi(k)$) for the Ce L_{III} Os L_{III} and As K edges of $\text{CeOs}_4\text{As}_{12}$ at $T = 4$ K. The Ce scan is limited by the Ce L_{II} edge while the As scan is limited by the Os L_{III} edge. The upper (Ce) and lower (As) traces are off-set by ± 1.1 . b) Similar k -space data for the oxy-skutterudite, $\text{PrCu}_3\text{Ru}_4\text{O}_{12}$ near 4K.

III. DATA

A. Ce L_{III} edge in the As-skutterudites

The Ce L_{III} -edge r -space data [Fourier Transform (FT) of $k\chi(k)$] are shown in Fig. 3 as a function of temperature for the three samples; $\text{CeM}_4\text{As}_{12}$ ($M = \text{Fe, Ru, Os}$). Note that in EXAFS the peak positions are always shifted to lower r - in this case $\sim 0.2 \text{\AA}$, compared to the actual pair distance. The fast oscillatory function in this figure is the real part, R , of the FT.

The first shell of neighbors around the Ce atom is an icosahedron of twelve As atoms (see Fig. 1:Right); it produces the largest peak in Fig. 3, just below 3\AA . The EXAFS second shell peak is near 3.4\AA (actual distance $\sim 3.6 \text{\AA}$), and consists of 8 neighbors of Fe, Ru, or Os. The theoretical functions for the second neighbor Ru and Os backscatterers are doubly peaked, with the shorter peak under the main Ce-As peak and the longer peak plotted as a shoulder near 3.8\AA . The Ce-Fe theoretical function is singly peaked but smaller than the Ce-Ru and Ce-Os functions because of the lower atomic number of Fe. In addition, there is interference between the oscillatory

components for the first and second peak leading to the dip near 3.5 Å; this makes it difficult to compare the data from the three samples without detailed fits.

At low temperature, the structure is well ordered, the Ce-As pair distribution width is small and the EXAFS amplitude is large. As temperature increases from 4 to 300 K, the pair distributions broaden rapidly for all three samples, resulting in a decreasing amplitude for each peak, with much of the drop in amplitude occurring by 200 K, and only $\sim 30\%$ remaining at 300K.

B. L_{III} edges for the oxy-skutterudites

For the oxy-skutterudites, the environment about the L_n atoms is very similar to that around Ce, as discussed above. There are 12 O first-neighbors and 8 Ru second neighbors. The main difference is the third neighbor L_n -Cu peak which occurs near 3.4 Å; there is no corresponding peak for the As-skutterudites. The L_{III} edge data for the lanthanide atoms La, Pr, and Nd are plotted in Fig. 4; the general shape is very similar to that for the As-skutterudites, but the first L_n -O peak has a shorter bond length and occurs near 2.3 Å on the EXAFS plot (actual distance is near 2.63 Å) while the L_n -Ru peak is near 3.0 Å. The dip at ~ 2.7 Å is again due in part to interference between the first two peaks.

The data in Fig. 4 show a weaker T dependence than the corresponding data for the Ce L_{III} edge plotted in Fig. 3. However, the unit cell is smaller for the oxy-skutterudites and the effective spring constants to the various neighbors are accordingly somewhat larger; consequently a weaker T dependence was expected. However, the temperature dependence for the L_{III} edges is much stronger than for the Cu or Ru K edge data in these samples.

C. Cage atom edges (As, Fe, Ru, Os) in As-skutterudites

The arrangement of As atoms can be viewed as six nearly square rings in the unit cell (Fig. 1:Left), which face in either the x , y , or z direction. Since the As atoms are not at the center of the cubic substructure like the Ce atom, there is less local symmetry about this site, which results in more shells of neighbors with lower degeneracies. The first shell of atoms around As contains two Fe, Ru, or Os neighbors at approximately 2.4 Å. This, together with two As neighbors near 2.5 Å form the first EXAFS peak plotted near 2 Å in the Supplement, Fig. S2. The next peak near 3 Å is a sum of a single As-Ce peak and an As-As peak with four neighbors. See Supplement for details about the further neighbor shells.

The Fe, Ru, and Os atoms make up the cubic network of their respective compounds. Data for $\text{CeFe}_4\text{As}_{12}$ and $\text{CeOs}_4\text{As}_{12}$ samples are from 4–300 K, while the data set for $\text{CeRu}_4\text{As}_{12}$ are from 4–330 K. The environment

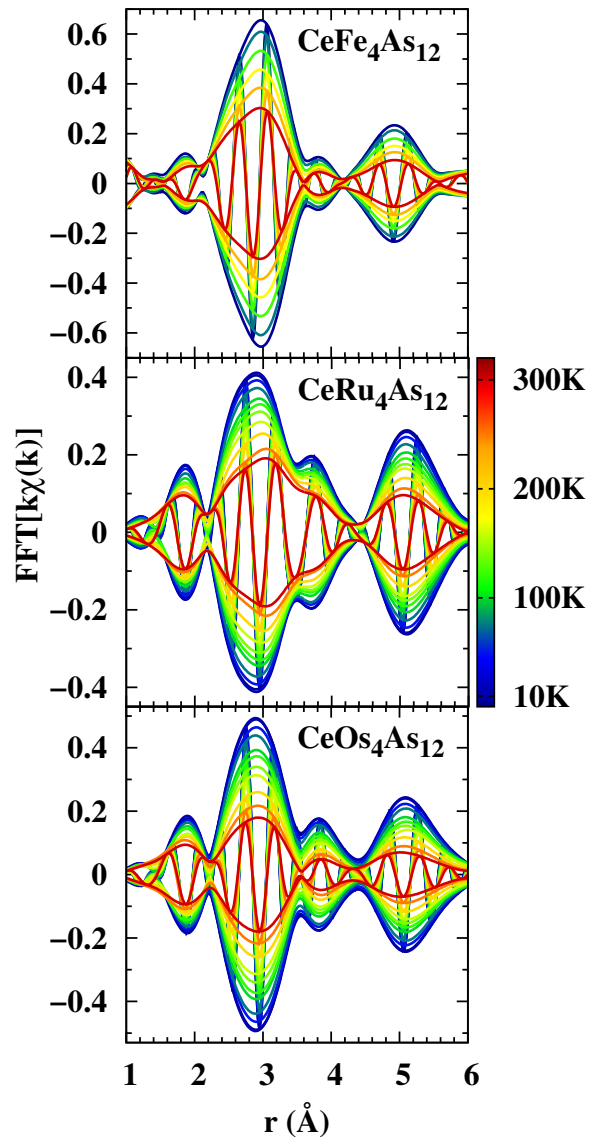


FIG. 3: (Color on-line) Temperature dependence, from 4 to 300 K, of the r -space data (FT of $k\chi(k)$) at the Ce L_{III} edge for $\text{CeM}_4\text{As}_{12}$ ($M = \text{Fe, Ru, Os}$) samples. The largest peak around 2.9 Å is the first As neighbor. Here and in following r -space plots the fast oscillation is the real part, R , of the FT; the amplitude function is $\pm\sqrt{R^2 + I^2}$ where I is the imaginary part (not plotted) of the FT. FT range: 3.5–9.8 Å $^{-1}$.

around the M atom site is very similar for all three edges; the first shell around the M site consists of 6 As atoms and produces the first EXAFS peak near 2 Å (see Fig. S1 in the Supplement). This M -As peak is very similar for each sample and has a relatively weak temperature dependence indicating a stiff bond. The next small peak near 3.3 Å, corresponds to a shell of two Ce atoms. The second large peak near 3.7–3.8 Å is the sum of 12 As at

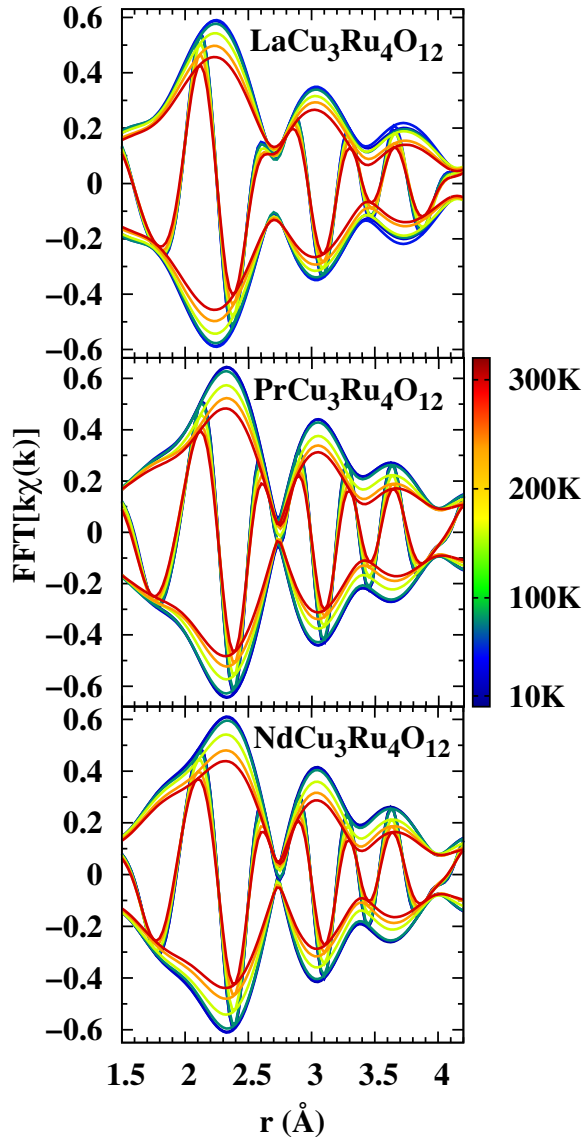


FIG. 4: (Color on-line) Temperature dependence of the r -space data at the lanthanide L_{III} edges for $LnCu_3Ru_4O_{12}$, $Ln = La, Pr, Nd$, from 4 to 300 K. The largest peak around 2.3 Å is the first O neighbor. The second neighbor peak (Ln -Ru) is near 3.0 Å and partially overlaps the first peak. FT ranges: La, 3.5–9.2 Å⁻¹; Pr and Nd, 3.5–10.0 Å⁻¹. Note the similar shape and behavior for the three samples.

~ 4.1 Å and 6 Fe, Ru, or Os atoms at approximately 4.2 Å. Further details are provided in the Supplement.

	a (Å)	x	y
CeFe ₄ As ₁₂	8.289	0.1543	0.3445
CeRu ₄ As ₁₂	8.500	0.1495	0.3499
CeOs ₄ As ₁₂	8.519	0.1485	0.3485
LaCu ₃ Ru ₄ O ₁₂	7.478	0.1762	0.3054
PrCu ₃ Ru ₄ O ₁₂	7.463	0.175	0.305
NdCu ₃ Ru ₄ O ₁₂	7.456	0.1717	0.2984

TABLE I: Lattice parameters and fractional site positions ($x, y, 0$) for the As or O atom in the $Im\bar{3}$ space group for CeM_4As_{12} ($M = Fe, Ru, Os$)¹³ and $LnCu_3Ru_4O_{12}$ ($Ln = La, Pr, Nd$)^{18,32}; accurate x and y parameters for O in the Pr sample are not available, and we use approximate values from Ref. 22. For the rare earths, the x, y, z parameters are 0, 0, 0 and the M atoms are located at $\frac{1}{4}, \frac{1}{4}, \frac{1}{4}$. In the oxy-skutterudites, Cu is located at $\frac{1}{2}, 0, 0$.

D. Cu and Ru K edge data for the oxy-skutterudites

For the oxy-skutterudites we do not have oxygen EXAFS to compare with the As EXAFS in the As samples, as the O K edge is at a very low energy. However, we have Cu K edge data which are presented in Fig S3 in the supplement; Cu is located at the center of the O₄ ring. These results show that the short Cu-O bond (near 1.6 Å) has a very weak T -dependence indicating very stiff Cu-O bonds and highly correlated motions of the Cu and O atoms.

In the oxy-skutterudites the Ru atoms form the cubic network, similar to the M atoms for the As-skutterudites. The r -space data for the Ru K edge are shown as a function of temperature in Fig. S4 in the supplement. There are six O nearest neighbor atoms which form the peak in the EXAFS data near 1.6 Å. The second neighbor peak near 2.8 Å is mostly Ru-Cu with a small Ru- Ln contribution while the peak near 3.4 Å is the Ru-Ru peak. These further neighbor peaks have stronger T -dependencies as expected. Further details are provided in the Supplement.

IV. DATA ANALYSIS

A. Detailed Crystal Structure

Details for the space group $Im\bar{3}$ ¹³ are provided in Table I for the three As-skutterudite and three oxy-skutterudite samples. The a parameter is the length of the sides of the cubic structure shown in Fig. 1. Note that the CeFe₄As₁₂ unit cell is somewhat smaller than for the CeRu₄As₁₂ and CeOs₄As₁₂ samples. Also, by changing the x and y fractional positions for the As atom, the As or O ring can be changed from a square (when $x+y = 0.5$) into a slightly more rectangular structure; we'll ignore this tiny effect in most of the discussion. However the CuO₄ rings in the

oxy-skutterudites are slightly more rectangular than the As_4 rings.

B. General Fitting & Constraints

Using the space group parameters given in Table I theoretical EXAFS functions were calculated for each pair of atoms using the program FEFF8.5³³. The data were then fit in r -space to a sum of these EXAFS functions; in principle, there are three parameters per atom-pair - amplitude, position (r) and the width σ , of the pair distribution function. Constraints must be included as otherwise there would be too many free parameters, as discussed by Stern³⁴.

In the following fits, the amplitudes and relative pair distances were constrained to be consistent with the known crystal structure as follows: the ratios of the amplitudes for each atom pair were constrained to the ratio of the coordination numbers; one amplitude was allowed

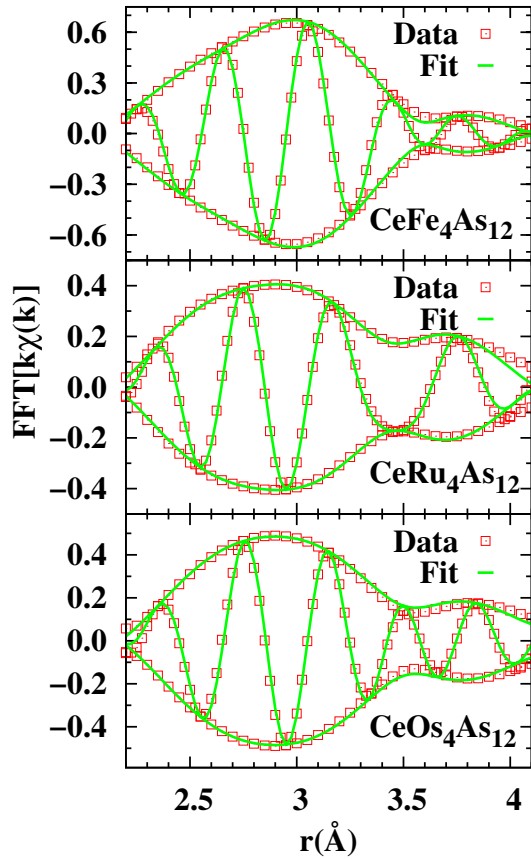


FIG. 5: (Color on-line) Fit of the Ce L_{III} edge data using a sum of theoretical functions for $\text{Ce}M_4\text{As}_{12}$ ($M = \text{Fe}, \text{Ru}, \text{Os}$) at 4 K. The fit ranges were 2.3–5.4, 2.4–4.0, and 2.3–5.6 Å for the Fe, Ru and Os samples respectively. Note that the fits to the longer As neighbors for the Fe and Os samples are not plotted on this scale.

to vary at low temperatures to determine the parameter S_o^2 and then was held constant for fits as a function of T . This is an important constraint because σ , and amplitude are strongly correlated. The ratios of the pair distances were also initially constrained to the lattice structure, with one distance parameter allowed to vary to compare with diffraction. One final parameter to be determined is ΔE_o - the difference between the experimentally determined edge energy (energy at half step height) and the energy at which $k = 0$ in the theory. Since there is a correlation between bond lengths (pair distances) and E_o , the parameter ΔE_o is determined at low temperatures where the amplitude is largest at high k in the k -space data, and then fixed for fits at higher temperatures.

C. Rattler Behavior

1. Ce L_{III} edge results; As-skutterudites

The Ce L_{III} edge data for $\text{CeFe}_4\text{As}_{12}$ (see Fig. 3) were fit using a k -range of 3.5–9.8 \AA^{-1} in $k\chi$ over an r -range of 2.3–5.4 Å using five theoretical functions calculated using FEFF8³³. The first shell of neighbors around the Ce atom in $\text{CeFe}_4\text{As}_{12}$ contains twelve As atoms at a distance of 3.129 Å while the next shell contains eight Fe atoms at 3.589 Å. Two longer As neighbors 5.201 Å and 5.582 Å with degeneracies twenty-four and twelve respectively, plus a multiscattering (MS) path with distance

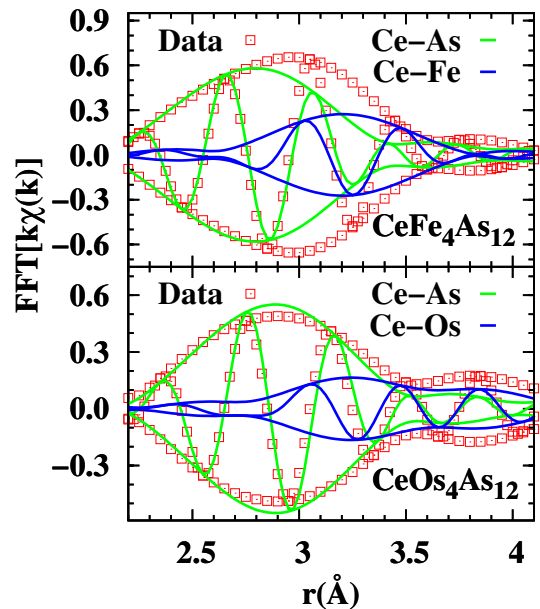


FIG. 6: (Color on-line) Details of the fits (Fig. 5) for the Fe and Os arsenide samples, showing the relative amplitudes and phase for the first (Ce-As - green) and second (Ce-Fe or Ce-Os - blue) neighbor pairs. Note the difference in the phase for the two cases and the change in the interference.

4.544 Å were included. This MS path corresponds to the scattering path Ce-As-Fe-Ce. Several weaker multiscattering paths were not included in the fit due to their very low EXAFS amplitude and long distance. The number of parameters fit was eight, far less than the number of independent parameters, sixteen, estimated from Stern's criteria³⁴.

For CeRu₄As₁₂, the Ce *L*_{III} edge data were fit using a *k*-range of 3.5–9.8 Å⁻¹ over an *r*-range of 2.4–4.0 Å using two theoretical functions for the nearest neighbor As atoms (3.234 Å) and the second neighbor Ru atoms (3.681 Å). For this sample, fits over the longer *r*-range used for the Fe and Os samples were not good and in the comparisons between these samples we will primarily consider only the first two neighbors. For these fits, only three parameters were varied; Stern's criteria gives 9.4 independent parameters. Note that the larger lattice parameter, *a*, results in increased distances between neighbors in the Ru and Os samples compared to the Fe sample. The fits for CeOs₄As₁₂ data were similar to those for the Fe edge data but included two MS paths instead of one. The FT and fit ranges were: *k*-range, 3.6–9.8 Å⁻¹; fit range, 2.3–5.6 Å. An example of a fit at 4 K up to ~ 4 Å is shown in Fig. 5 for the three samples.

An important detail is that one cannot obtain good parameters for the first peak in the Ce *L*_{III} edge data without including the second peak, which partially overlaps the first peak. This is shown explicitly for two samples in Fig. 6. For CeFe₄As₁₂, the oscillatory functions for the two peaks are in phase and constructive interference occurs, while for CeOs₄As₁₂ the oscillatory functions are partially out of phase and some destructive interference occurs.

The pair distances obtained in these fits agree quite well with diffraction,¹³ with a small contraction at low *T* (see Table II in supplement); consequently, we do not discuss the pair distances further. From the fits as a function of temperature we extracted $\sigma^2(T)$ for the Ce-As and first Ce-*M* pairs. These are plotted in Fig. 7. For Ru and Os, σ^2 at 4 K is the same for the first two neighbors, i.e., the vibrations are essentially isotropic at low *T*, while for the Fe sample there is a static off-set for the second neighbor – approximately 0.002 Å². The most important result is that $\sigma^2(T)$ increases faster with *T* for the second peak for all samples. This is surprising if one assumes a stiff cubic unit cell; then vibrations along *x*, *y*, or *z* are equivalent and in that case one would expect the Ce vibrations to be isotropic. Instead, the larger amplitude vibrations of the Ce-*M* pairs at 300 K means that either the *M* atoms are moving significantly at 300 K or there is some anharmonicity in the vibrations at 300 K as suggested for PrOs₄Sb₁₂,³⁵ - or a combination of these effects. We address this stiffness and possible non-isotropic vibrations in the discussion section.

The $\sigma^2(T)$ results were then fit to an Einstein model under the stiff cage assumption; in this case the reduced mass is just the mass for Ce. Rattler-like behavior is apparent for Ce from the large amplitude vibrations and

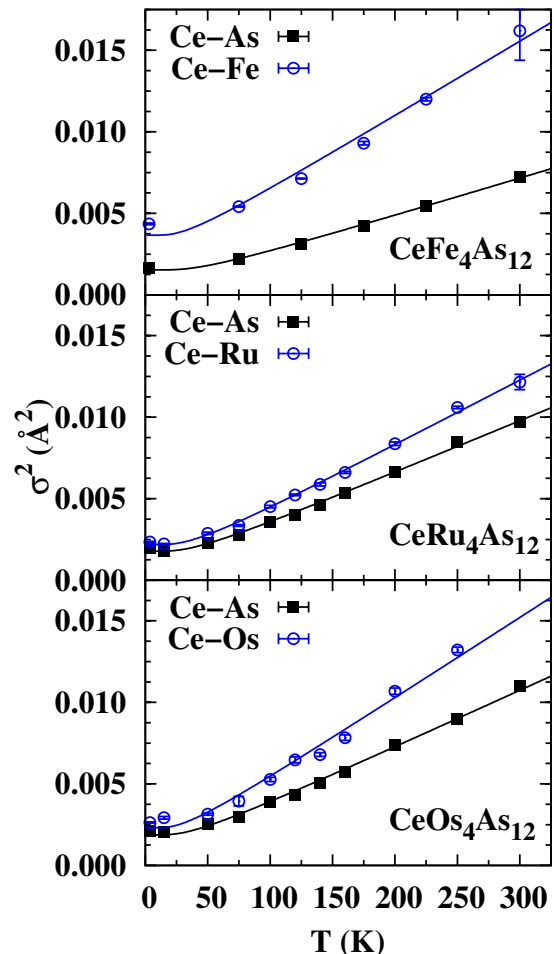


FIG. 7: (Color on-line) $\sigma^2(T)$ for the first two neighbors about Ce, and Einstein model fits for CeM₄As₁₂ (*M* = Fe, Os, Ru) samples; Ce-As₁ are the lower traces in each case. Note the different vertical scale for each plot. In this and subsequent plots of σ^2 we use the following convention: first neighbor pair - black square; second neighbor pair - blue circle.

the low Einstein temperatures (θ_E) for the Ce-As pair, tabulated in Table II; this pair is stiffest (largest θ_E) for the Fe sample. The values of θ_E for the various atom pairs confirm the qualitative discussion above. Note that for the Ru sample, the anisotropy of the Ce vibration is quite small - i.e., the difference in σ^2 at 300 K for the two pairs is small and the Einstein temperatures are nearly equal. The anisotropy increases for the Os sample and is largest for the Fe sample; this sample has the largest difference in θ_E for the first and second neighbors. Except for the Ce-Fe peak, the static off-sets σ_{static}^2 are all very small - consistent with zero local distortions at 4 K. For the Fe sample, it is not clear if the small static off-set for the second neighbor is just some residual strain in the sample or an indication of some structural distortion - somewhat similar to that recently observed in NdOs₄Sb₁₂.²⁴

CeFe ₄ As ₁₂	θ_E (K)	σ_{static}^2 (\AA^2)
Ce-As	124	0.0002
Ce-Fe	87	0.0017
CeRu ₄ As ₁₂	θ_E (K)	σ_{static}^2 (\AA^2)
Ce-As	104	0.0001
Ce-Ru	101	0.0001
CeOs ₄ As ₁₂	θ_E (K)	σ_{static}^2 (\AA^2)
Ce-As	101	0.0002
Ce-Os	84	0.0002
LaCu ₃ Ru ₄ O ₁₂	θ_E (K)	σ_{static}^2 (\AA^2)
La-O	139	0.0022
La-Ru	175	0.0015
La-Cu	152	0.0017
PrCu ₃ Ru ₄ O ₁₂	θ_E (K)	σ_{static}^2 (\AA^2)
Pr-O	135	0.0010
Pr-Ru	163	0.0003
Pr-Cu	149	0.0004
NdCu ₃ Ru ₄ O ₁₂	θ_E (K)	σ_{static}^2 (\AA^2)
Nd-O	128	0.0016
Nd-Ru	160	0.0003
Nd-Cu	135	0.0000

TABLE II: Ce L_{III} Einstein-model fit results for $\text{Ce}M_4\text{As}_{12}$ ($M = \text{Fe}, \text{Ru}, \text{Os}$), top, and $\text{LnCu}_3\text{Ru}_4\text{O}_{12}$ ($\text{Ln} = \text{La}, \text{Pr}, \text{Nd}$), bottom. Estimated absolute errors are ± 20 K due to systematic errors; relative errors between fits are < 8 K; uncertainty in $\sigma_{\text{static}}^2 \sim 0.0004 \text{\AA}^2$. Note: many values of σ_{static}^2 are consistent with $\sigma_{\text{static}}^2 = 0$.

2. Ln edge results: Oxy-skutterudites

The analysis of the data for the oxy-skutterudites parallels that for the As skutterudites, with the exception that there are no results for the As skutterudites to compare with the Cu edge data and we have no O K edge data. Since the results for the rattler atoms La, Pr, and Nd are distinctly different from the corresponding Ce results in the As skutterudites, we provide details about these fits.

The La edge data for $\text{LaCu}_3\text{Ru}_4\text{O}_{12}$ were fit using a k -range of $3.5\text{-}9.7 \text{\AA}^{-1}$ and an r -range of $2\text{-}4 \text{\AA}$. We used seven theoretical functions to fit the data including four single scattering paths; the 12-fold degenerate La-O peak at 2.6\AA , the 8-fold degenerate La-Ru peak at 3.2\AA , the 6-fold degenerate La-Cu peak at 3.7\AA , and the 24-fold degenerate La-O peak at 4.7\AA . Multiscattering paths at 3.9\AA , 4\AA , and 4.9\AA were also included. In the fit the multiscattering peaks positions were allowed to vary slightly, and their σ 's were constrained to be a weighted sum of the La-O and La-Ru σ 's. The Pr edge data were fit identically but with a k -range of $3.5\text{-}10 \text{\AA}^{-1}$, an r -range of $1.75\text{-}4.25 \text{\AA}$, and slightly different constraints on the multiscattering functions.

For the fit of the Nd edge the k -range was $3.5\text{-}10 \text{\AA}^{-1}$ and the r -range was set to $1.2\text{-}4.5 \text{\AA}$. In this case seven standards were again used, including the same first four neighbors as for the La and Pr fits. The multiscattering

peaks at 3.9\AA and 4\AA were also used, but a multiscattering peak at 5.1\AA was used instead of the weak peak at 4.9\AA . For this edge the first Nd-O distance was allowed to vary independently of the rest of the unit cell. Examples of fits for the rare earth edge of all three samples at 25 K are shown in Fig. 8. Except for the Nd-O distance which is $\sim 0.04 \text{\AA}$ longer, the results for position agree well with diffraction and a comparison is given in the Supplement. For the Nd sample the x and y parameters for the As position are slightly smaller than for the La and Pr samples (see Table I); if we used the La x and y parameters for Nd, then there would be very little disagreement for the Nd-O bond length.

We now focus on the functions $\sigma^2(T)$, extracted from these fits. For the La, Pr, and Nd edges we again use an Einstein model to model $\sigma^2(T)$ under the assumption that the rattler atoms vibrate independently inside a nearly rigid cage of Ru and O atoms. Fits of the data were carried out for the first three neighbors about the rattler atom and are plotted, together with the data, in Fig. 9; the fit-results are also tabulated in Table II. We

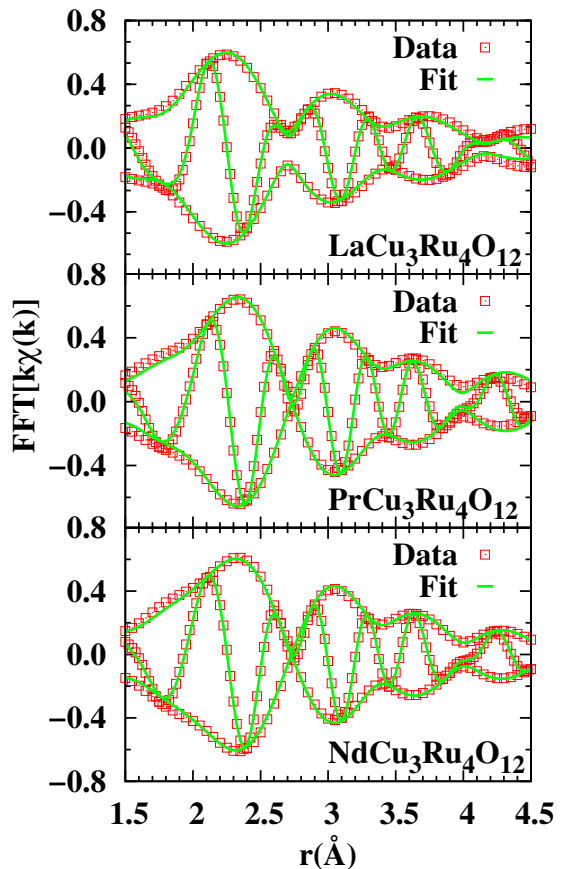


FIG. 8: (Color on-line) Fit of the Ln L_{III} edge data using a sum of theoretical functions for $\text{LnCu}_3\text{Ru}_4\text{O}_{12}$ ($\text{Ln} = \text{La}, \text{Pr}, \text{Nd}$) at 6 K. The fit ranges were $2\text{-}4$, $1.75\text{-}4.25$, and $1.2\text{-}4.5 \text{\AA}$ for the La, Pr, and Nd samples respectively.

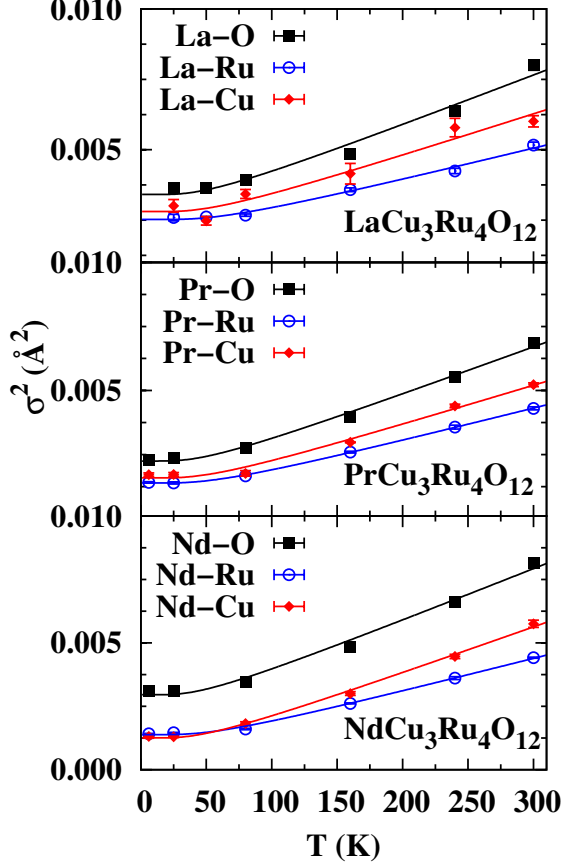


FIG. 9: (Color on-line) $\sigma^2(T)$ for the first three neighbors about the Ln atom in $LnCu_3Ru_4O_{12}$ ($Ln = La, Pr, Nd$) samples, plus Einstein model fits; Ln -O pairs have the highest slopes while the Ln -Ru have the lowest slopes in each case. Same color convention as in Fig. 7 but here and in following plots, we use red diamonds for the third neighbors.

observe that the second neighbor (Ln -Ru bond is significantly stiffer than that of the first neighbor (Ln -O bond, which is in stark contrast to the Ce edge results for the CeM_4As_{12} samples. We also see that $\sigma^2(T)$ for (Ln -O and (Ln -Cu have similar slopes and Einstein temperatures. The comparable value of $\sigma^2(T)$ for these two pairs suggests that if the cage is not rigid, the oxygen ring with the copper atom at its center, moves as a nearly rigid unit.

V. CAGE ATOMS

3. Fe K, Ru K, Os L_{III} & As K edges

In this section, we probe the stiffness of the cage structure for the As-skutterudites, formed from the M and As atoms out to the third or fourth neighbors. To include

all the edges and pairs is a somewhat lengthy analysis - the details of these fits are provided in the supplement.

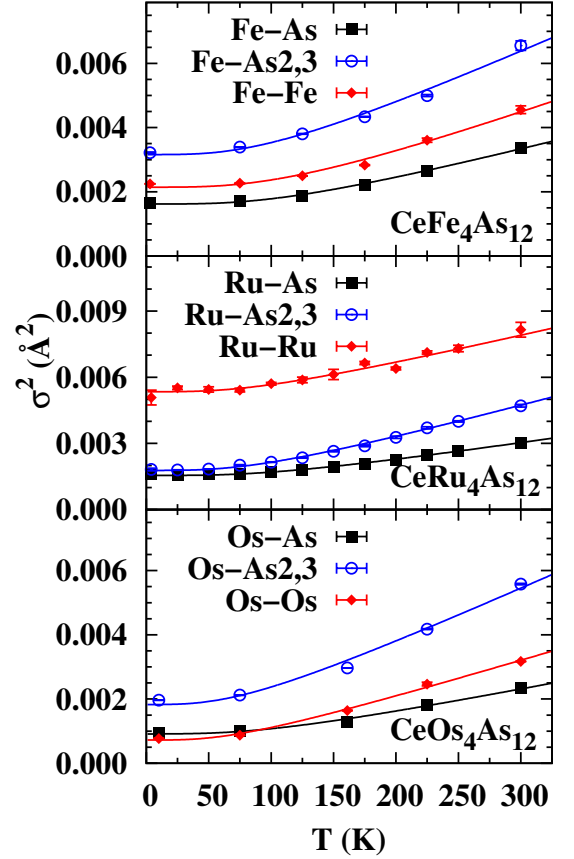


FIG. 10: (Color on-line) $\sigma^2(T)$ for several atom pairs from the fits of the M edge data for CeM_4As_{12} ($M = Fe, Os, Ru$), and correlated Debye model fits to these results (solid lines). Note the different vertical scale for the Ru sample (middle plot).

From the fits, the $\sigma^2(T)$ functions were again extracted for each pair up to 300 K. The results for the M edges (Fe, Ru, Os) are plotted in Fig. 10; note that these data show a rather small increase with T compared to the Ce data. Thus the M -edge results for the first few neighbors support the assumption that the cage formed of M and As atoms is relatively stiff. The σ^2 values for the nearest neighbor are smallest for the central Os atom due to its larger atomic mass compared to the Ru and Fe atoms. The Ru-Ru pair for $CeRu_4As_{12}$ also has a large static offset, indicative of some additional disorder in that sample.

The $\sigma^2(T)$ results were fit to a correlated Debye model using the reduced mass of the atom pair. The fits are plotted in Fig. 10 as solid lines and the parameters are tabulated in Table III. Some values of σ_{static}^2 are slightly negative but within our uncertainties for this parameter. With the exception of the Ru-Ru pair and possibly the second Fe-As pair, the small values of σ_{static}^2 are consis-

tent with zero, i.e., no significant static distortions for most pairs.

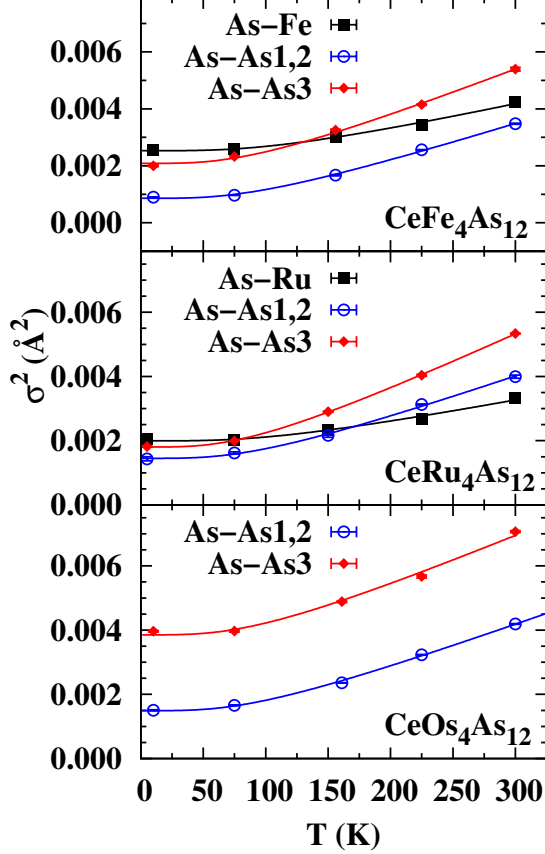


FIG. 11: (Color on-line) σ^2 as a function of temperature at the As K edge for several atom pairs in CeM_4As_{12} ($M = \text{Fe, Os, Ru}$), plus correlated Debye model fits (solid lines). Note the different vertical scales for the three plots and the large static distortion for As-As₃ in $CeOs_4As_{12}$.

The correlated Debye temperatures, θ_{cD} , are large, which indicates stiff atom pairs. Also, the first M -As pair consistently has the strongest bond, parametrized by a larger value of θ_{cD} , which is expected, due to the shorter bond length. In general θ_{cD} decreases with increasing pair-distance; the exception is for Fe-Fe, but this is the pair for which there is strong destructive interference with a MS peak (see Supplement). Consequently the value of θ_{cD} for Fe-Fe is likely too high.

$CeFe_4As_{12}$	θ_{cD} (K)	σ_{static}^2 (\AA^2)
Fe-As1	467	-0.0001
Fe-As2,3	388	0.0010
Fe-Fe	519	-0.0004
As-Fe	475	0.0008
As-As1,2	385	-0.0011
As-As3	384	-0.0002
As-As4	376	0.0044

$CeRu_4As_{12}$	θ_{cD} (K)	σ_{static}^2 (\AA^2)
Ru-As1	444	0.0002
Ru-As2,3	404	-0.0003
Ru-Ru	372	0.0033
As-Ru	471	0.0007
As-As1,2	384	-0.0004
As-As3	375	-0.0006
As-As4	387	0.0003

$CeOs_4As_{12}$	θ_{cD} (K)	σ_{static}^2 (\AA^2)
Os-As1	436	-0.0002
Os-As2,3	360	-0.0002
Os-Os	268	-0.0001
As-As1	375	-0.0004
As-As3	396	0.0016

TABLE III: Fit results using a correlated Debye model to describe $\sigma^2(T)$, for the Fe, Ru, Os, and As edges in CeM_4As_{12} ($M = \text{Fe, Ru, Os}$). Except for the Fe-Fe peak, estimated absolute errors are ± 40 -50 K for θ_{cD} due to systematic errors; relative errors are $\sim \pm 10$ -15 K. Estimated errors for the static distortion, σ_{static}^2 , are $\pm 0.0004 \text{ \AA}^2$. Note that most of the static off-set values are consistent with $\sigma_{static}^2 = 0$. For the Os sample interference between As-Os and the first As-As peak made the results unstable; to obtain good results for As-As1, the parameters for the As-Os peak were constrained to the values obtained for the Os-As peak from the Os edge analysis. Similarly the parameters for the weak As-Ce peak for each sample were constrained to the corresponding values from the Ce L_{III} edge results.

Similar results were obtained from fits of the As edge data. The $\sigma^2(T)$ results are presented in Fig. 11 along with the correlated Debye fits (solid lines); the results are also tabulated in Table III. We do not include the As-Ce peak as this small peak is better defined from the Ce L_{III} -edge data. For the first few neighbors, σ^2 is small at low temperatures and grows slowly with T . The temperature dependence is weakest for the Fe sample which has the smallest unit cell.

For the As K edge results, the nearest neighbor As-Fe and As-Ru bonds are stiffer than for further neighbor As-As pairs. The θ_{cD} values for As-Fe and As-Ru agree within errors, with the corresponding values for Fe-As and Ru-As from the M edges.

For the Os sample the strong interference between the first two peaks (As-Os and As-As1) results in unstable fits. To obtain consistent results for the As-As1 peak (second neighbor peak) we have used the value of σ for Os-As peak from the Os edge results, to constrain σ for the nearest neighbor As-Os peak in the As data fit; this leads to stable consistent results for As-As1. Note that all As-As pairs (and in all samples) have about the same

θ_{cD} values - ~ 380 K; however, because there are many overlapping peaks above 4 Å the tails of these peaks overlap the third As-As3 peak and the fit parameters for this peak may be less reliable.

The static off-sets (σ_{static}^2) are also shown in Table III; they are small and in most cases consistent with $\sigma_{static}^2 \sim 0$. One exception is for the fourth shell (As-As3 pair) in the $CeOs_4A_{12}$ sample, for which σ_{static}^2 is ~ 0.0016 Å²; however, even this value is not large. The other exception is the negative value for As-As1 in the Fe sample; this value is outside our usual errors for σ_{static}^2 and $\sigma^2(4K)$ is too small for this peak. It likely arises from the large amount of interference between overlapping peaks.

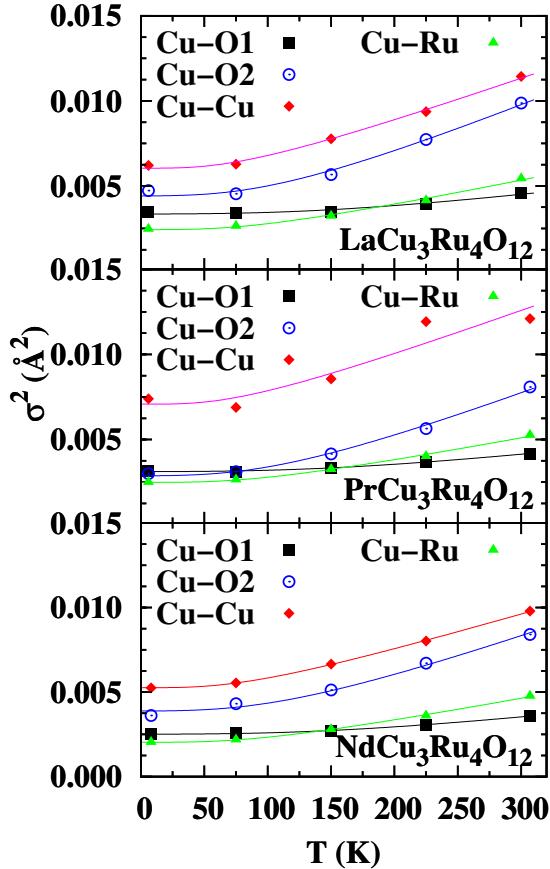


FIG. 12: (Color on-line) $\sigma^2(T)$ for several atom pairs from the fits of the Cu edge data for $LnCu_3Ru_4O_{12}$ ($Ln = La, Pr, Nd$), and correlated Debye model fits to these results (solid lines). Third neighbors Cu-Ru - green triangles; fourth neighbors Cu-Cu - red diamonds.

In summary, for the As skutterudites the first few neighbor atom pairs within the cage are quite stiff, with characteristic temperatures of order 380-450 K. Further neighbor pairs have lower values for θ_{cD} but are still relatively stiff. The small static contribution to σ^2 for the first few neighbors indicates that there is little static disorder from local strain. These results show that the cage structure formed of M and As atoms is relatively stiff.

However, it should not be considered to be completely rigid when considering rattling motions, as the characteristic temperatures for cage-atom pairs are only a factor of 4 higher than the rattler Einstein temperatures.

4. Cu and Ru K edges

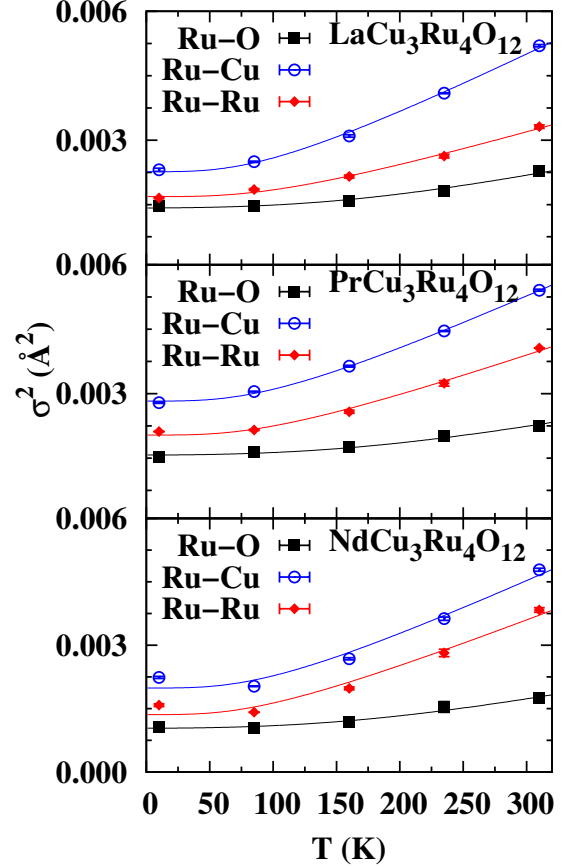


FIG. 13: (Color on-line) $\sigma^2(T)$ for several atom pairs from the fits of the Ru edge data for $LnCu_3Ru_4O_{12}$ ($Ln = La, Pr, Nd$), and correlated Debye model fits to these results (solid lines).

Details about the fits of the Cu and Ru edge data are provided in the supplement and are similar to the fits for the cage atoms in the As-skutterudites. Here we show the $\sigma^2(T)$ results extracted from those fits for the first four neighbors, and fit them using a correlated-Debye model. The data and fits are shown in Fig. 12, and the fit-results are tabulated in Table IV. We find that Cu-O1 is an extremely stiff bond, further indicating that the CuO_4 ring moves as a unit with the Cu at its center. This does not rule out the possibility that the Cu atom may have some movement perpendicular to the oxygen ring plane. The fact that the Cu-O2 and the Cu-Cu peaks have softer effective spring constants is an indication that

some transverse vibration might be taking place. We see further evidence for the ring's movement as a unit, from the parallel slopes of $\sigma^2(T)$ for the Cu-O2 and Cu-Cu peaks. The O2 and Cu neighbors correspond to atoms in neighboring rings, and thus indicate that the neighboring rings also display this joint movement. Interestingly, even though the slopes of the fits are the same for the Cu-Cu and Cu-O2, the Debye temperatures are significantly different, because we have used *different* reduced masses. However, if the ring moves as a whole, the same slopes mean comparable force constants between a Cu atom and the atoms in a neighboring ring, and the simple reduced mass model may not be appropriate; i.e., one may need to consider the entire mass of a rigid ring. Thus, the higher values of θ_{cD} for Cu-O2 compared to Cu-Cu, *only* reflect the difference in reduced masses for Cu/O2 and Cu/Cu atom pairs. We explore this issue more in Sec. VIA.

LaCu ₃ Ru ₄ O ₁₂	θ_{cD} (K)	σ_{static}^2 (Å ²)
Cu-O1	823	0.0008
Cu-O2	520	-0.0008
Cu-Ru	423	0.0003
Cu-Cu	367	0.0030
Ru-O	982	-0.0007
Ru-Cu	433	0.0001
Ru-Ru	506	0.0003
PrCu ₃ Ru ₄ O ₁₂	θ_{cD} (K)	σ_{static}^2 (Å ²)
Cu-O1	858	0.0007
Cu-O2	540	-0.0022
Cu-Ru	442	0.0004
Cu-Cu	363	0.0039
Ru-O	1026	-0.0005
Ru-Cu	453	0.0008
Ru-Ru	466	0.0005
NdCu ₃ Ru ₄ O ₁₂	θ_{cD} (K)	σ_{static}^2 (Å ²)
Cu-O1	858	0.0001
Cu-O2	559	-0.0010
Cu-Ru	442	-0.0001
Cu-Cu	399	0.0024
Ru-O	1012	-0.0010
Ru-Cu	447	-0.0001
Ru-Ru	433	-0.0003

TABLE IV: Fit results using a correlated Debye model to describe $\sigma^2(T)$, for the Cu and Ru edges in $LnCu_3Ru_4O_{12}$ ($Ln = La, Pr, Nd$). Except for the Cu-O1 and Ru-O peaks, estimated absolute errors are ± 40 -50 K for θ_{cD} due to systematic errors; relative errors are $\sim \pm 10$ -15 K. Estimated errors for the static distortion, σ_{static}^2 , are ± 0.0004 Å². Again most of the static off-sets are consistent with zero off-set. The parameters for the weak Cu- Ln and Ru- Ln peaks for each sample were constrained to the corresponding values from the $Ln L_{III}$ edge.

To fit the $\sigma^2(T)$ data for the Ru-edge data we again used a correlated-Debye model. The Debye fits for the three most relevant atom-pairs are shown in Fig. 13 and the results of these fits are shown in Table IV. We see that the Ru-O bond is very stiff, suggesting that the oxy-

gen atoms are most likely constricted to motion within the CuO₄ plane. The Ru-Ru bond is stiffest for the Nd data and softest for the La data, but all bonds are comparable. Note that the Ru-Cu fit results are consistent with the corresponding results for Cu-Ru from the Cu edge data.

VI. DISCUSSION

A. Effective Spring Constants

The results from the analysis of $\sigma^2(T)$ are usually given in terms of Einstein or correlated Debye temperatures – but these quantities depend on the assumed reduced mass. As discussed in Sec. IA, the slope of the $\sigma^2(T)$ plot at high T is a direct measure of the effective spring constant K. This has been known since the early work on EXAFS²⁷ but is rarely reported;^{36,37} however, in comparing atomic vibrations it is very useful to compare the force constants. These are obtained by extrapolating our Einstein or correlated Debye fits to high T and obtaining the inverse slope on the $\sigma^2(T)$ plots. These effective spring constants should not be confused with the actual harmonic spring between a pair of atoms, particularly for the weaker springs, as they include contributions from the surrounding network. Such effective spring constants are tabulated in Table V for the first few atom pairs. The stiffest constants for the oxy-skutterudites are the Ru-O and Cu-O bonds while the bonds between the rattler and its neighbors are weaker. Similarly for the arsenides; the strongest bonds are the nearest neighbor M -As and As-As bonds while the bonds to the Ce rattler atom are weaker. In all cases the effective spring constants connecting rattler atoms to their nearest neighbors are only a factor of 2-4 smaller than the strongest spring constants between cage atoms.

It is useful to consider how assumptions about the reduced mass and the choice of Einstein vs correlated Debye model, affect the Einstein/Debye temperatures, the static off-set parameters and the effective spring constants. To explore these issues we use the $\sigma^2(T)$ data for the Ce-As peak in CeRu₄As₁₂, which has a large number of temperature points. We consider three reduced masses in amu units: Ce in a rigid cage, $M = 140$; Ce connected to a rigid As₄ ring that acts as a massive atom ($4M_{As}$), $M = 95.5$; and the simple reduced mass of a Ce-As pair, $M = 48.8$. As expected θ_E and θ_{cD} vary as $1/\sqrt{M}$. For a given value of M, θ_{cD} is about 44 % larger than θ_E . The most important point to note is that the static off-set (σ_{static}^2) changes with the choice of M and decreases as the reduced mass decreases; for our data, σ_{static}^2 becomes negative for the smaller reduced masses. However, σ_{static}^2 does not differ much between Einstein and correlated Debye models. These results are summarized in Table VI. The estimated effective spring constants, K_{eff} , are also tabulated for each case; K_{eff} decreases very slightly with decreasing M, but is independent of the choice of Einstein

Pair	CeFe ₄ As ₁₂ (eV/Å ²)	CeRu ₄ As ₁₂ (eV/Å ²)	CeOs ₄ As ₁₂ (eV/Å ²)
Ce-As	3.72	2.70	2.46
Ce- <i>M</i>	1.88	2.15	1.73
M-As1	8.22	9.85	10.84
M-As2	3.540	5.94	5.01
M-M	5.71	4.57	5.24
As-As	6.52	6.10	5.96

	LaCu ₃ Ru ₄ O ₁₂ (eV/Å ²)	NdCu ₃ Ru ₄ O ₁₂ (eV/Å ²)	PrCu ₃ Ru ₄ O ₁₂ (eV/Å ²)
(<i>Ln</i> -O)	4.78	4.17	4.59
(<i>Ln</i> -Ru)	7.50	6.50	6.65
(<i>Ln</i> -Cu)	5.71	4.67	5.51
Cu-O1	8.84	9.61	9.62
Cu-O2	2.72	3.15	2.96
Cu-Ru	5.47	5.98	5.95
Cu-Cu	3.37	3.81	3.15
Ru-O	12.41	13.34	13.47
Ru-Cu	5.73	6.09	6.27
Ru-Ru	9.74	7.17	8.27

TABLE V: Table showing the experimentally calculated effective spring constants K_{eff} for the filled skutterudites $\text{CeM}_4\text{As}_{12}$ and oxy-skutterudites $\text{LnCu}_3\text{Ru}_4\text{O}_{12}$, obtained from the inverse slope of the σ^2 plot extrapolated to high T. Relative errors for Einstein (rattler) modes are $< 10\%$; however because of the high values of θ_{cD} for the rest of the structure, the high temperature extrapolations must extend well above 300 K and consequently, the estimated systematic errors for K_{eff} are much higher; of order 20% for lower $\theta_{cD} < 500$ K, and 30% for the higher $\theta_{cD} \sim 1000$ K are difficult to estimate. Note that in general, the effective spring constants for atom pairs defining the cage are significantly stiffer than the springs between the rattler atom and its neighbors.

or correlated Debye model. The goodness of fit parameter χ^2 is lowest when using the middle reduced mass (95.5) for each model, and increases 30-40 % when using the larger or smaller reduced mass. This supports the idea that the As_4 ring is quite rigid and is involved in the rattling motion; however, we did not explore the mass dependence in detail. For the middle mass, the Einstein model is slightly better.

M	Ce (140)	Ce-As ₄ (95.5)	Ce-As (48.8)
θ_E (K)	104	124	167
σ_{static}^2 (Å ²)	.0001	-.0002	-.0009
θ_{cD} (K)	148	179	241
σ_{static}^2 (Å ²)	.0001	-.0002	-.0009
K_{eff} (eV/Å ²)			
Einstein	2.70	2.61	2.42
Debye	2.71	2.62	2.44

TABLE VI: A summary of Einstein temperatures θ_E and correlated Debye temperatures, θ_{cD} , and corresponding static off-sets, σ_{static}^2 , using different assumptions for the reduced mass of the rattler. The second part of the table shows that the spring constants, extracted from a high T extrapolation, are reduced slightly as the reduced mass decreases, but are independent of the choice of Einstein or correlated Debye model.

B. Summary of New Results and Previous Measurements

For all of the skutterudites investigated, the structure observed in EXAFS is very close to that observed in diffraction - see Table II above and Tables SII, SIII, SV, and SVII-SVIII in the supplement. The only small disagreement is for the x and y positions of the O atoms in the Nd sample; the Cu-O distances are slightly shorter (~ 0.03 Å) than calculated from the diffraction results while the Nd-O bond is approximately 0.04 Å longer. This suggests a slightly smaller CuO_4 ring with a more rectangular shape.

Important differences are observed in comparing the σ^2 results and relative spring constants for the first few neighbors about the rare earth rattler atoms. The most striking result is that for the oxy-skutterudites, the second neighbor pair, *Ln*-Ru, has a stiffer force constant than the first neighbor pair *Ln*-O. In contrast, in the arsenides, the second neighbor force constant is slightly smaller than that for the first neighbor. The apparently weaker *Ln*-O bond is particularly surprising since O normally forms strong bonds - and the Cu-O and Ru-O bonds are indeed very stiff.

A second, less obvious conclusion is that the As_4 and CuO_4 rings are nearly rigid units and their suspension within the skutterudite structure is anisotropic. This is best understood when viewing the structure as a skutterudite rather than as a double perovskite^{15,17} with tilted octahedra. The rings are suspended in the structure via Ru-O or *M*-As bonds which are indeed quite stiff - but these bonds are nearly perpendicular to the rings - see Fig. 14, and thus only provide stiff restoring forces for motion perpendicular to the rings. For motion towards the rattler atoms however, (left/right in Fig. 14) the restoring forces provided by the Ru-O or *M*-As bonds are much weaker and are given by $K \cos^2(\theta)$ where θ is the angle between the displacement direction of interest (here towards rattler) and the spring direction, and K is the Ru-O or *M*-As spring constant. For these sys-

tems, $\cos^2(\theta)$ can be ~ 0.1 for vibrations towards the rattler atom; the effective spring constant is then smaller than any direct spring constants in the structure. There are also spring constants between different As_4 rings but these also provide only a small restoring force for motion towards the rattler.

An important difference for the oxy-skutterudites is that, compared to the size of the unit cell, the CuO_4 ring is relatively larger than the pnictide ring (As_4) and $\cos^2(\theta)$ is consequently smaller for the oxy-skutterudites. For example, for $\text{CeFe}_4\text{Sb}_{12}$, $\cos^2(\theta)$ is 0.113 while for $\text{PrCu}_3\text{M}_4\text{O}_{12}$, it is 0.043. Thus, this suggests that the rings can also act as “rattlers” in some directions; such motion will also couple to the acoustic modes and contribute to a reduced thermal conductivity. The rattler-ring system therefore forms weakly connected chain linkages along the x , y , and z directions within a stiffer framework; vibrations within this linkage should not be considered local modes. In addition, the effective mass is probably not that of the atom pair under consideration but instead likely includes the ring mass. If the ring structures can move easily towards/away from the rattler, then both the rigid cage model and the simple reduced mass assumption are poor approximations. However if the ring mass were very large, the rigid cage model would be more applicable. The discussion at the end of Sec. VIA suggests that using a combination of the Ce atom and the As_4 ring for the reduced mass, may be a significantly better approximation.

Other local structure studies of these systems are very limited. To our knowledge, there are no EXAFS studies of the As skutterudites. The behavior for the rattler-nearest-neighbor pair in the arsenides presented here, is between that for phosphides and antimonides³⁸ but in that earlier work we did not investigate the temperature dependence for the second neighbors. The same difference in slope for the first and second neighbors was observed recently in three antimonides as noted in the introduction,²⁴ but the focus there was on the unusual static distortions for the second neighbors in two of the materials.

Nitta *et al.*^{23,39} have studied a number of Sb skutterudites but focused only on the first neighbors. A similar study of phosphide skutterudites has been carried out by Mizumaki *et al.*,⁴⁰ but again, only the first neighbors were considered. Thus there are no second neighbor results with which to compare, even in related systems. For all the first neighbor results for the As and oxy-skutterudites reported here, we find much less static distortion for the nearest neighbors about the rare earth atom; this arises in part from the fact that there is interference in the k -space EXAFS between the first and second neighbor pairs, and in r -space the real and imaginary components can show destructive or constructive interference - as shown for example in Fig. 6. Ignoring the second neighbors will change the parameters for the first peak. For the systems considered here, and including the second rattler neighbor in the analysis, we find

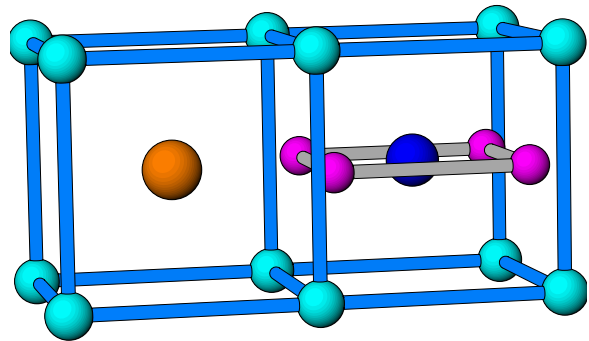


FIG. 14: (Color on-line) Two sub-cubes of the unit cell showing a rattler atom and a CuO_4 ring within the cubes formed of Ru (or Fe and Os) atoms. Note that the bond between the Ru (blue) and O (small purple) atoms is nearly perpendicular to the plane of the CuO_4 ring and hence for motion towards the rattler, the restoring force on the CuO_4 ring from the Ru atoms is very small. Similar results apply to the As_4 ring in the As-skutterudites.

no evidence for any off-center behavior as proposed by Nitta *et al.*^{23,39} for several Sb skutterudites.

For the oxy-skutterudites, one EXAFS study investigated the environment about Ru in several samples at 77 K, and showed that the local structure about Ru was consistent with diffraction,¹⁸ as we find here. In their analysis they used a somewhat smaller value of the S_o^2 parameter (0.72) for the Ru K edge and their values of σ^2 are correspondingly slightly smaller than reported here. Finally, Zheng *et al.*⁴¹ investigated the related compound $\text{CaCu}_3\text{Ti}_4\text{O}_{12}$ using a range of techniques including EXAFS and PDF analysis, but focused on possible Ca/Cu antisite disorder at room temperature.

VII. CONCLUSIONS

The EXAFS results agree well with the structure and space group obtained from diffraction for all samples; the only slight disagreement is in the position of the O atoms in $\text{NdCu}_3\text{Ru}_4\text{O}_{12}$ leading to a longer Nd-O bond by ~ 0.04 Å and a more rectangular shape for the CuO_4 ring. The EXAFS results for the Nd sample are more consistent with the oxygen x and y parameters for the Pr and La samples.

The most important new results from this study pertain to the local thermal vibrations and the effective spring constants extracted from these measurements. First, the ring structures also appear to be quite stiff and likely can be considered to be nearly independent, rigid units within the structure. Also, many of the effective spring constants between first and second neighbor pairs in the cage structure are indeed quite stiff but not stiff enough to support a completely rigid cage approximation.

Note that if the skutterudite lattice ($\text{Cu}_3\text{Ru}_4\text{O}_{12}$ for

oxy-skutterudites and M_4As_{12} for the arsenides) were really rigid, the vibrations of the rattler atom would be isotropic - same σ^2 for first and second neighbor pairs - but it is not. For the arsenides, the second neighbor pairs Ce-*M* have a weaker spring constant than for the first neighbor bond, Ce-As. Even more surprising is that for the oxy-skutterudites the second neighbor spring constant, for *Ln*-Ru, is significantly stiffer than for the nearest neighbor *Ln*-O bond.

A further evaluation of the structure shows that the restoring forces on the As_4 and CuO_4 rings are not isotropic. There are stiff restoring forces for motion perpendicular to the rings but weak forces for motion parallel to the rings, particularly in the direction of the rattler. We suggest that the rings also act as rattlers for some directions of motion and are coupled to the rare earth rattlers. This sets up a coupled network of overlapping weak and strong springs, and the resulting vibration amplitudes are not straight forward to evaluate. Preliminary analysis using a 1-D model with four atoms in the unit cell, shows that one can in fact model the unusual difference between the arsenide skutterudites and the oxy-skutterudites. This work will be published separately.⁴²

Finally, determining the value of the static component, σ_{static}^2 , for the disorder of the nearest neighbor pair about the rattler, is not straightforward. One needs to at least include the second neighbor peak in the fits and the value of σ_{static}^2 depends on the assumed reduced mass when fitting to an Einstein model.

Acknowledgments

This work was supported under NSF grant DMR1005568. We thank Jacob Stanley for his help in the early stages of this project. The experiments were performed at SSRL, operated by the DOE, Division of Chemical Sciences. Research at UCSD (materials synthesis and characterization) was supported by the U. S. Department of Energy, Office of Basic Energy Sciences, Division of Materials Sciences and Engineering under Award Grant no. DE-FG02-04-ER46105. Research at ILTSR (growth of CeM_4As_{12} crystals and characterization) was supported by the Polish National Science Centre within Grant No. 2011/01/B/ST3/05685.

-
- * Current address: National High Magnetic Field Laboratory - Florida State University, Tallahassee, FL 32310-3706
- ¹ B. C. Sales, in Handbook on the Physics and Chemistry of the Rare Earths, edited by L. Eyring, J. K. A. Gschneider, and G. H. Lander (Elsevier Science Publishing Co., New York, 2003), Vol. 33, Chap. 211, pp. 1–34.
 - ² M. B. Maple, Z. Henkie, R. E. Baumbach, T. A. Sayles, N. P. Butch, P.-C. Ho, T. Yanagisawa, W. M. Yuhasz, R. Wawryk, T. Cichorek, and A. Pietraszko, *J. Phys. Soc. Jpn.*, Suppl. A **77**, 7 (2008).
 - ³ M. B. Maple, R. E. Baumbach, J. J. Hamlin, P. C. Ho, L. Shu, D. E. MacLaughlin, Z. Henkie, R. Wawryk, T. Cichorek, and A. Pietraszko, in Properties and Applications of Thermoelectric Materials, NATO Sci. Peace Sec. Series B: Physics and Biophysics, edited by V. Zlatic and A. C. Hewson (Springer, Netherlands, 2009), pp. 1–18.
 - ⁴ M. B. Maple, *Physica B* **404**, 2924 (2009).
 - ⁵ B. C. Sales, D. Mandrus, B. C. Chakoumakos, V. Keppens, and J. R. Thompson, *Phys. Rev. B* **56**, 15081 (1997).
 - ⁶ V. Keppens, D. Mandrus, B. C. Sales, B. C. Chakoumakos, P. Dai, R. Coldea, M. B. Maple, D. A. Gajewski, E. J. Freeman, and S. Bennington, *Nature* **395**, 876 (1998).
 - ⁷ H. Sugawara, S. Osaki, M. Kobayashi, T. Namiki, S. R. Saha, Y. Aoki, and H. Sato, *Phys. Rev. B* **71**, 125127 (2005).
 - ⁸ R. E. Baumbach, P.-C. Ho, T. A. Sayles, M. B. Maple, R. Wawryk, T. Cichorek, T. Pietraszko, and Z. Henkie, *J. Phys. Condens. Matter* **20**, 075110 (2008).
 - ⁹ R. E. Baumbach, P.-C. Ho, T. A. Sayles, M. B. Maple, R. Wawryk, T. Cichorek, T. Pietraszko, and Z. Henkie, *Proc. Natl. Acad. Sci.* **105**, 17307 (2008).
 - ¹⁰ R. Wawryk, Z. Henkie, A. Pietraszko, T. Cichorek, L. Kepinski, A. Jezierski, J. Kaczkowski, R. E. Baumbach, and M. B. Maple, *Phys. Rev. B* **84**, 165109 (2011).
 - ¹¹ N. R. Dilley, E. J. Freeman, E. D. Bauer, and M. B. Maple, *Phys. Rev. B* **58**, 6287 (1998).
 - ¹² G. S. Nolas, M. Kaeser, R. T. Littleton, and T. M. Tritt, *Appl. Phys. Lett.* **77**, 1855 (2000).
 - ¹³ Z. Henkie, M. B. Maple, A. Pietraszko, R. Wawryk, T. Cichorek, R. E. Baumbach, W. M. Yuhasz, and P.-C. Ho, *J. Phys. Soc. Jpn.*, Suppl. A **77**, 128 (2008).
 - ¹⁴ B. H. Yan, L. Muchler, X.-L. Qi, S.-C. Zhang, and C. Felser, *Phys. Rev. B* **85**, 165125 (2012).
 - ¹⁵ M. A. Subramanian and A. W. Sleight, *Solid State Sci.* **4**, 347 (2002).
 - ¹⁶ A. P. Ramirez, G. Lawes, D. Li, and M. A. Subramanian, *Solid State Commun.* **131**, 251 (2004).
 - ¹⁷ A. N. Vasil'ev and O. S. Volkova, *Low Temp Phys.* **33**, 895 (2007).
 - ¹⁸ S. G. Ebbinghaus, A. Weidenkaff, and R. J. Cava, *J. Solid State Chem.* **167**, 126 (2002).
 - ¹⁹ S. Tanaka, N. Shimazui, H. Takatsu, S. Yonezawa, and Y. Maeno, *J. Phys. Soc. Jpn.* **78**, 024706 (2009).
 - ²⁰ N. Büttgen, H.-A. K. von Nidda, W. Kraetschmer, A. Günther, S. Widmann, S. Riegg, A. Krimmel, and A. Loidl, *J. Low Temp Phys* **161**, 148 (2010).
 - ²¹ N. Hollmann, Z. Hu, A. Maignan, A. Gunther, L.-Y. Jang, A. Tanaka, H.-J. Lin, C. T. Chen, P. Thalmeier, and L. H. Tjeng, *Phys. Rev. B* **87**, 155122 (2013).
 - ²² U. Schwingenschlogl, V. Eyert, and U. Eckern, *Chem Phys Lett* **370**, 719 (2003).
 - ²³ K. Nitta, Y. Omori, D. Kikuchi, T. Miyanaga, K. Takegahara, H. Sugawara, and H. Sato, *J. Phys. Soc. Jpn.* **77**, 063601 (2008).
 - ²⁴ T. Keiber, F. Bridges, R. E. Baumbach, and M. B. Maple, *Phys. Rev. B* **86**, 174106 (2012).
 - ²⁵ J. L. Feldman, P. Dai, T. Enck, B. C. Sales, D. Mandrus, and D. J. Singh, *Phys. Rev. B* **73**, 014306 (2006).

- ²⁶ S. Tsutsui, H. Kobayashi, Y. Yoda, H. Sugawara, C. Sekine, T. Namiki, I. Shirovani, and H. Sato, *Hyperfine Interact* **206**, 67 (2012).
- ²⁷ B. K. Teo, EXAFS: Basic Principles and Data Analysis (Springer-Verlag, New York, 1986), dOI=10.1007/978-3-642-50031-2.
- ²⁸ C. H. Booth and F. Bridges, *Physica Scripta* **T115**, 202 (2005).
- ²⁹ See <http://lise.lbl.gov/RSPAK>.
- ³⁰ J. A. Victoreen, *J. Appl. Phys.* **20**, 1141 (1949).
- ³¹ Y. Jiang, F. Bridges, N. Sundaram, D. P. Belanger, I. E. Anderson, J. F. Mitchell, and H. Zheng, *Phys. Rev. B* **80**, 144423 (2009).
- ³² M. Labeau, B. Bochu, J. C. Joubert, and J. Chenavas, *J Solid State Chem* **33**, 257 (1980).
- ³³ A. L. Ankudinov, B. Ravel, J. J. Rehr, and S. D. Conradson, *Phys. Rev. B* **58**, 7565 (1998).
- ³⁴ E. A. Stern, *Phys. Rev. B* **48**, 9825 (1993).
- ³⁵ K. Kaneko, N. Metoki, H. Kimura, Y. Noda, T. D. Matsuda, and M. Kohgi, *J. Phys. Soc. Jap.* **78**, 074710 (2009).
- ³⁶ P. Fornasini, *J. Phys.: Condens. Matter* **13**, 7859 (2001).
- ³⁷ A. Sanson, *Chem. Mater.* **26**, 3716 (2014).
- ³⁸ D. Cao, F. Bridges, P. Chesler, S. Bushart, E. D. Bauer, and M. B. Maple, *Phys. Rev. B* **70**, 094109/1 (2004).
- ³⁹ K. Nitta, Y. Omori, T. Miyanaga, K. Takegahara, H. Sugawara, D. Kikuchi, and H. Sato, *J. Phys. Soc. Jpn.* **82**, 044801/1 (2013).
- ⁴⁰ M. Mizumaki, S. Tsutsui, T. Uruga, H. Tanida, D. Kikuchi, H. Sugawara, and H. Sato, *J. Phys. Soc. Jpn.* **80**, 074603/1 (2013).
- ⁴¹ J.-C. Zheng, A. I. Frenkel, L. Wu, J. Hanson, W. Ku, E. S. Bozin, S. J. L. Billinge, and Y. Zhu, *Phys. Rev. B* **81**, 144203 (2010).
- ⁴² T. Keiber and F. Bridges (unpublished).